

Sensitivity of a Spherical Resonant Gravitational Wave Detector

Florian Dubath,¹ Jérôme Extermann,² and Luciano Gottardi³

¹ *Département de Physique Théorique, Université de Genève,
24 quai Ernest-Ansermet, CH-1211 Genève 4*

² *GAP - Biophotonics, Université de Genève,
20 rue de l'Ecole de Médecine, CH-1211 Genève 4*

³ *SRON National Institute for Space Research,
Sorbonnelaan 2, 3584 CA Utrecht, Netherlands*

Abstract

We present a numerical analysis to simulate the response of a spherical resonant gravitational wave detector and to compute its sensitivity. We compute both the sensitivity of each different transducers and the sensitivity obtain from a coherent analysis of the whole set of transducers. We use our model to work out the transfer function and the strain sensitivity for different designs of spherical detectors. In particular we present the case of 1 meter radius bulk and hollow spheres equipped with transducer in TIGA configuration.

I. INTRODUCTION

Direct detection of gravitational waves (GW) is still an unachieved goal. The sensitivity improvement of single detectors [1], to achieve the first detection, goes in parallel with the set-up of detector networks to perform real GW astronomy [2]. To that purpose, future GW detectors should be able to track GW arrival directions. Due to their symmetry, spherical resonant detectors are natural GW ‘telescope’ candidates. Moreover, such detectors are based on the same technology as resonant bars and can benefit of the decades of experience gain by the GW community with this kind of experimental setup.

The main limitation when dealing with resonant detectors, is the small bandwidth compared with laser interferometers [3].

Great progress have been made using the tuning of the electrical mode [4] which allows to enlarge the bandwidth from few Hz to the order of 100 Hz around the resonance frequency. A possible way to further enlarge the bandwidth consists of monitoring other resonance frequencies of the antenna. In the case of a cylindrical detector this strategy is not convenient since the coupling of the n -th longitudinal mode fall of as $(2n + 1)^{-2}$. However for a sphere the next mode quintuplet is tightly coupled to GW. Monitoring these modes is possible using many transducers, tuned at different frequencies. One can also use double transducers able to amplify two frequencies [6]. We have to stress that both issues are experimental challenges.

Another technical problem resides in the fact that big cryogenic resonant spheres with high quality factor are difficult to build and to cool. One can partially bypass this problem using hollow spheres.

In order to compare different GW detectors it is important to be able to compute the strain sensitivities. This is the goal of this paper: we compute the noise spectrum and the sensitivity of each transducer placed on the sphere, taking into account all the internal noise sources. We treat each transducer output separately even if in the case of TIGA configuration [5] it is possible to (linearly) combine these signals in order to obtain the mode channels. Our analysis can be compared with existent sensitivity computation [7] but we stress the fact that each transducer is affected by all the noises (mechanical, electrical and SQUID noises) from all the transducers. Therefor we build a matrix model including all the noises (except SQUID current noises which do not back-react on the sphere.)

The rest of the paper is organized as follows. After describing in section II the dynamics of the different parts of a spherical GW detector, we present in section III the noise sources of the detector. In section IV compute the detector's response to a GW and its sensitivity. The last section is dedicated to different examples. In particular we work out the strain sensitivities for 1[m] radius bulk and hollow spheres, with 6 or 12 transducers.

II. DESCRIPTION OF SPHERICAL RESONANT GW DETECTORS

A. The modes of a sphere

The vibrational motion of a rigid body can be split into eigen-modes. For a sphere there are two families of modes: the toroidal ones and the spheroidal ones [9]. Each mode can be described as a forced damped harmonic oscillator, which means that the j -th mode [18] amplitude z_j satisfies in Fourier space the equation

$$m_s \left(\omega_{s,j}^2 - \omega^2 + i \frac{\omega \omega_{s,j}}{Q_{s,j}} \right) \tilde{z}_j(\omega) = \tilde{F}_j(\omega) , \quad (1)$$

where m_s is the sphere's mass, $\omega_{s,j}$ is the j -th mode eigen-frequency, $Q_{s,j}$ its quality factor and $\tilde{F}_j(\omega)$ the Fourier component of the forcing. The forcing of the mode is due to a stochastic (Langevin) force and to external forces. The stochastic force corresponds to the thermal excitation of the sphere mode. Among the external forces we retain only the tidal forces induced by GW and forces due to the coupling of the mode with the transducers.

B. Transducer

To give a clear presentation of the noises and the sensitivity we need a full model for the transducer. We use capacitive transducers, see figure 1, based on the miniGRAIL one [10], composed by one resonator coupled to a dc-SQUID with input transformer, where the SQUID is described as a linear current amplifier [11].

On a mathematical footing each transducer (a mechanical resonator with its read-out) will be modeled by a set of $p = 3$ coupled differential equations, driven by the specific intrinsic noises and its coupling to the sphere. In Fourier space each transducer and each

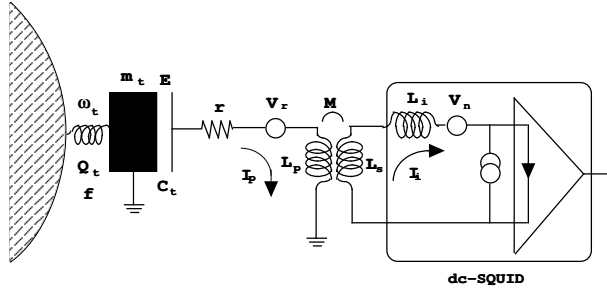


FIG. 1: The transducer model. We show only the variables we use.

read-out are described by the equation set

$$\begin{pmatrix} m_t \left(\omega_t^2 - \omega^2 + i \frac{\omega \omega_t}{Q_t} \right) & -iE/\omega & 0 \\ E & r + i(\omega L_p - \frac{1}{(\omega C_t)}) & -iM\omega \\ 0 & -iM\omega & i\omega(L_s + L_i) \end{pmatrix} \begin{pmatrix} \tilde{q} \\ \tilde{I}_p \\ \tilde{I}_i \end{pmatrix} = \begin{pmatrix} \tilde{f} \\ \tilde{V}_r \\ \tilde{V}_n \end{pmatrix} \quad (2)$$

where m_t , ω_t , Q_t are the resonators mass, eigen-frequency and quality factor, E is the electric field in the capacitor C_t formed with the resonator, r the transformers resistance, L_i , L_p , L_s the inductances of the SQUID input coil, primary and secondary of the transformer, and M the mutual inductance of the transformer; see figure 1. \tilde{q} is the transducers position [12], \tilde{I}_p , \tilde{I}_i are the currents into the transformer and the SQUID, and \tilde{I}_i is the measured quantity. Finally, \tilde{V}_r and \tilde{V}_n are the voltages corresponding to the intrinsic noise and \tilde{f} is the sum of the thermal force and the coupling to the sphere's modes. When we use more than one transducer an index is added to all this quantities.

C. Coupling transducers to the modes of the sphere

It is important to note that generally a transducer is coupled with a subset of the five sphere modes and therefore the presence of transducers provides an indirect coupling between the different modes. Reciprocally, different transducers are coupled through the sphere's modes. Therefore, the total noise spectrum of a given transducer has a contribution from the intrinsic noises of the other transducers.

We call θ_k, ϕ_k the location of the k -th transducer. At this point of the sphere's surface, the $j = \{n, l, m\}$ -th spheroidal mode induces a radial displacement

$$\alpha_{nl}(R_s)Y_{lm}(\theta_k, \phi_k) \equiv \alpha_j B_{jk} \quad (3)$$

where $\alpha_j \equiv \alpha_{nl}(R_s)$ is the radial eigen-function evaluated at the sphere's surface, and Y_{lm} is a spherical harmonic. This equation defines the pattern matrix B_{jk} . Using this matrix we complete the equation of motion found in [5] by adding dissipative terms [10]. The coupling between the sphere's modes and the transducers is then given (in Fourier space) by

$$\tilde{F}_j = \tilde{F}_j^{\text{noise+GW}} + \sum_k \alpha_j B_{jk} \left(\left(\omega_{t,k}^2 + i \frac{\omega \omega_{t,k}}{Q_{t,k}} \right) m_{t,k} \tilde{q}_k - \tilde{f}_k^{\text{noise}} \right) \quad (4)$$

$$\tilde{f}_k = \tilde{f}_k^{\text{noise}} + m_{t,k} \omega^2 \sum_j B_{jk} \alpha_j \tilde{z}_j. \quad (5)$$

We obtain a set of $(J + pN)$ coupled equations, with J the number of modes taken into account and N the number of transducers.

D. Bulk sphere example

As an example, we present in all details a model with only the spheroidal quadrupole modes of the sphere ($J = 5$, $l = 2$), and with $N = 6$ capacitive transducers placed in the TIGA configuration [19] [5]. Note that we can write the system of $(J + pN)$ equations in the same form independently of the number of modes and transducers.

Collecting the equations (1,2,3,4) and (5) we obtain a description of the entire detector as

$$\underbrace{\begin{pmatrix} \mathbf{S} & \mathbf{C}_1 & 0 \\ \mathbf{C}_2 & & \\ \hline 0 & & \mathbf{T} \end{pmatrix}}_{\mathbf{Z}} \begin{pmatrix} \tilde{\mathbf{z}} \\ \tilde{\mathbf{q}} \\ \tilde{\mathbf{I}}_p \\ \tilde{\mathbf{I}}_i \end{pmatrix} = \underbrace{\begin{pmatrix} \mathbb{1}_5 & -\alpha \mathbf{B} & 0 & 0 \\ 0 & \mathbb{1}_6 & 0 & 0 \\ 0 & 0 & \mathbb{1}_6 & 0 \\ 0 & 0 & 0 & \mathbb{1}_6 \end{pmatrix}}_{\mathbf{A}} \begin{pmatrix} \tilde{\mathbf{F}}^{\text{noise+GW}} \\ \tilde{\mathbf{f}}^{\text{noise}} \\ \tilde{\mathbf{V}}_r \\ \tilde{\mathbf{V}}_n \end{pmatrix} \quad (6)$$

where $\tilde{\mathbf{z}} = \begin{pmatrix} \tilde{z}_1 \\ \vdots \\ \tilde{z}_5 \end{pmatrix}$, $\tilde{\mathbf{q}} = \begin{pmatrix} \tilde{q}_1 \\ \vdots \\ \tilde{q}_6 \end{pmatrix}$, and so on for the other variables.

\mathbf{S} is a 5×5 diagonal sub-matrix given by the left hand side (LHS) of (1), \mathbf{T} is a $3 \cdot 6 \times 3 \cdot 6$ sub-matrix with structure given by the LHS of (2) (each number in (2) is now a 6×6 diagonal matrix). The matrices \mathbf{C}_1 and \mathbf{C}_2 are 5×6 (resp. 6×5) sub-matrix read out of (4,5) [20] which describe the mechanical coupling between the spheroidal modes and the transducer

modes and are given by

$$\mathbf{C}_1 = -\alpha \mathbf{B} \text{Diag} \left(m_{t,k} (\omega_{t,k}^2 + i \frac{\omega \omega_{t,k}}{Q_{t,k}}) \right) \quad (7)$$

$$\mathbf{C}_2 = -\alpha \omega^2 \text{Diag}(m_{t,k}) \mathbf{B}^T . \quad (8)$$

III. DETECTOR NOISE DESCRIPTION

Starting from equation (6), knowing the forces and the voltage acting on the detector allows us to compute the sphere's modes $\tilde{\mathbf{z}}$, the displacement $\tilde{\mathbf{q}}$ of the transducer, and the currents $\tilde{\mathbf{I}}_p$ and $\tilde{\mathbf{I}}_i$. To do that we invert the \mathbf{Z} matrix and rewrite (6) as

$$\begin{pmatrix} \tilde{\mathbf{z}} \\ \tilde{\mathbf{q}} \\ \tilde{\mathbf{I}}_p \\ \tilde{\mathbf{I}}_i \end{pmatrix} = \underbrace{\mathbf{Z}^{-1} \mathbf{A}}_{\mathbf{G}} \begin{pmatrix} \tilde{\mathbf{F}}^{\text{noise+GW}} \\ \tilde{\mathbf{f}}^{\text{noise}} \\ \tilde{\mathbf{V}}_r \\ \tilde{\mathbf{V}}_n \end{pmatrix} \quad (9)$$

Mode amplitudes, transducer displacement and transformer currents are not directly measured and we are interested only in the N last lines of \mathbf{G} , giving the proportionality coefficients between forces (and voltages) and SQUID input currents $\tilde{\mathbf{I}}_i$.

We now work out the different noises contributions.

A. Noise description

We restrict ourself to the case where the disturbances $\mathbf{F}^{\text{noise}}$, $\mathbf{f}^{\text{noise}}$ and \mathbf{V}_r are only due to thermal excitations. In this case we can only access statistical property of these forces that is:

$$\langle F(t) \rangle = 0 \quad \langle V(t) \rangle = 0 , \quad (10)$$

$$\langle F(t)F(t') \rangle = A_0 \delta(t - t') \quad \langle V(t)V(t') \rangle = A_0^e \delta(t - t') . \quad (11)$$

Furthermore one can compute [13] that the coefficient A_0 takes the form

$$A_0 = 2k_B T m / Q \quad A_0^e = 2k_B T r . \quad (12)$$

where k_B is the Boltzmann constant, T is the thermodynamic temperature of the detector, and r the transformer resistance.

Using the definition of the side-sided spectral density of the force which is obtained through the autocorrelation

$$\langle F(t)F(t') \rangle = \frac{1}{2} \int \frac{d\omega}{2\pi} S_F(\omega) e^{-i\omega(t-t')} , \quad (13)$$

we obtain

$$\mathbf{S}_{F,j} = 4m_s \frac{k_B T}{Q_{s,j}} \quad (14)$$

$$\mathbf{S}_{f,k} = 4m_{t,k} \frac{k_B T}{Q_{t,k}} \quad (15)$$

$$\mathbf{S}_{V_r,k} = 4k_B T r_k \quad (16)$$

The SQUID has also intrinsic noises which can be split into voltage and current noises. The determination of these noises require the knowledge of the complete SQUID design. Therefore, we have to go beyond the description of subsection II B. In particular we need the shunt resistance $R_{sh,k}$ used to remove hysteresis, the washer inductance $L_{SQ,k}$, and $M_{SQ,k}$ the mutual inductance between the SQUID input and the washer, see fig. 2.

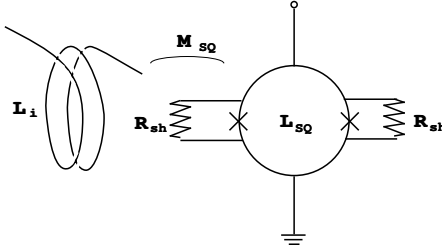


FIG. 2: SQUID detail. We show only the variables we use.

The SQUID voltage and current noises are, according to Clarke's model [11]

$$\mathbf{S}_{V_{n,k}} = 11 \frac{k_B T_{SQ,k}}{R_{sh,k}} \omega^2 M_{SQ,k} \quad (17)$$

$$\mathbf{S}_{W,k} = 16 \left(\frac{L_{SQ,k}}{M_{SQ,k}} \right)^2 \frac{k_B T_{SQ,k}}{R_{sh,k}} \quad (18)$$

where $T_{SQ,k}$ is the SQUID's effective temperature.

B. Noise matrix

The noise transducer outputs are proportional to the SQUID input current and thus given by

$$\tilde{\mathbf{I}}_i(\omega) = \mathbf{M}_i \mathbf{G}(\omega) \begin{pmatrix} \tilde{\mathbf{F}}^{\text{noise}} \\ \tilde{\mathbf{f}}^{\text{noise}} \\ \tilde{\mathbf{V}}_r \\ \tilde{\mathbf{V}}_n \end{pmatrix} (\omega) + \tilde{\mathbf{I}}_W(\omega) \equiv \mathbf{G}_I(\omega) \tilde{\mathbf{F}}(\omega) + \tilde{\mathbf{I}}_W(\omega) \quad (19)$$

where $\tilde{\mathbf{I}}_W(\omega)$ is the SQUID noise current and

$$\mathbf{M} = (0_{N,J} \ 0_{N,N} \ 0_{N,N} \ 1_N) \quad (20)$$

used in order to conserve only the SQUID input current and we have defined $\mathbf{G}_I(\omega) \equiv \mathbf{M}_i \mathbf{G}(\omega)$ to simplify the notation.

From this current we can compute the noises matrix \mathbf{S} , which is given by

$$\mathbf{S}^{\text{noise}} = \mathbf{I}_i(\omega) \mathbf{I}_i^\dagger(\omega) = \mathbf{G}_I \tilde{\mathbf{F}} \tilde{\mathbf{F}}^\dagger \mathbf{G}_I^\dagger + \mathbf{G}_I \tilde{\mathbf{F}} \tilde{\mathbf{I}}_W^\dagger + \tilde{\mathbf{I}}_W \tilde{\mathbf{F}}^\dagger \mathbf{G}_I^\dagger + \tilde{\mathbf{I}}_W \tilde{\mathbf{I}}_W^\dagger \quad (21)$$

The matrix $\tilde{\mathbf{F}} \tilde{\mathbf{F}}^\dagger$ is the correlation matrix of the different forces and voltages (Note that not all entries have the same units). Assuming that the different forces and voltage are only due to noises and are not-correlated this reduce to a diagonal matrix containing only autocorrelation

$$\mathbf{F} \mathbf{F}^\dagger = \text{Diag}(\mathbf{S}_F, \mathbf{S}_f, \mathbf{S}_{V_r}, \mathbf{S}_{V_n}) \quad (22)$$

The same argument leads to the cancellation of the $\tilde{\mathbf{F}} \tilde{\mathbf{I}}_W^\dagger$ and $\tilde{\mathbf{I}}_W \tilde{\mathbf{F}}^\dagger$ terms into (21) and to set

$$\tilde{\mathbf{I}}_W \tilde{\mathbf{I}}_W^\dagger = \text{Diag}(\mathbf{S}_W) \quad (23)$$

Therefore under the assumption that the different noises are not correlated the noise matrix (21) reduces to

$$\mathbf{S}^{\text{noise}} = \mathbf{G}_I \text{Diag}(\mathbf{S}_F, \mathbf{S}_f, \mathbf{S}_{V_r}, \mathbf{S}_{V_n}) \mathbf{G}_I^\dagger + \text{Diag}(\mathbf{S}_W) \quad (24)$$

IV. EFFECT OF A GW

The presence of a GW will manifest itself as a force acting on the sphere modes. We skip the computation (see [5]) and just note that in Fourier space the force acting on the j -th

mode is

$$\tilde{F}_j^{\text{GW}} = -\frac{1}{2}\omega^2 m_s \chi_j R_s \tilde{h}_j \quad (25)$$

where $\chi_j R_s$, the effective length of the mode, depends only on the multiplet (n) to which the mode belongs, and \tilde{h}_j is the projection of the (spatial part of the) GW tensor [21] on the j -th mode. Choosing the decomposition of the tensor on real matrix [12] we specify the form of $\tilde{\mathbf{h}}$ as

$$\tilde{\mathbf{h}} = \mathbf{T}_V \begin{pmatrix} \tilde{h}_+ \\ \tilde{h}_\times \end{pmatrix} \equiv \begin{pmatrix} \frac{\sqrt{3}}{2} \sin^2 \theta & 0 \\ -\frac{1}{2} \sin 2\theta \sin \phi & \sin \theta \cos \phi \\ \frac{1}{2} \sin 2\theta \cos \phi & \sin \theta \sin \phi \\ \frac{1}{2} (1 - \cos^2 \theta) \cos 2\phi & \cos \theta \sin 2\phi \\ -\frac{1}{2} (1 - \cos^2 \theta) \sin 2\phi & \cos \theta \cos 2\phi \end{pmatrix} \begin{pmatrix} \cos 2\psi & \sin 2\psi \\ -\sin 2\psi & \cos 2\psi \end{pmatrix} \begin{pmatrix} \tilde{h}_+ \\ \tilde{h}_\times \end{pmatrix} \quad (26)$$

where θ, ϕ give the arrival direction and ψ is the polarization angle [22].

The presence of a GW in a noise-free detector leads to an output signal given by the vector of SQUID input current

$$\mathbf{I}_{\text{sig}}(\omega) = \mathbf{G}_I(\omega) \begin{pmatrix} \tilde{\mathbf{F}}^{\text{GW}}(\omega) \\ \mathbf{0} \\ \mathbf{0} \\ \mathbf{0} \end{pmatrix} = \hat{\mathbf{G}}_I(\omega) \tilde{\mathbf{F}}^{\text{GW}}(\omega) = -\frac{1}{2}\omega^2 m_s R_s \chi \hat{\mathbf{G}}_I(\omega) \mathbf{T}_V \begin{pmatrix} \tilde{h}_+ \\ \tilde{h}_\times \end{pmatrix} \quad (27)$$

where we have assumed that all χ_j have the same value χ and we have defined $\hat{\mathbf{G}}_I$, the sub-matrix

$$\hat{\mathbf{G}}_I = \mathbf{G}_I \begin{pmatrix} 1_J \\ 0_{N,J} \\ 0_{N,J} \\ 0_{N,J} \end{pmatrix} = (0_{N,J} \ 0_{N,N} \ 0_{N,N} \ 1_N) \mathbf{G} \begin{pmatrix} 1_J \\ 0_{N,J} \\ 0_{N,J} \\ 0_{N,J} \end{pmatrix} \quad (28)$$

V. DETECTOR SENSITIVITY

The detector sensitivity is given by the comparison between the output due to the noise and the one due to a GW. Thus the sensitivity depend on the kind of analysis performed with the outputs from the N transducers.

A. Single transducer analysis

If we are looking only at the transducer $n^o k$ its noise spectral density is given by the diagonal component of (24) and is

$$\begin{aligned} S_{I_i^k} &= \mathbf{S}^{kk} = \sum_{\ell=1}^j |\mathbf{G}_{J+2N+k,\ell}|^2 \mathbf{S}_{F,\ell} + \sum_{\ell=1}^N |\mathbf{G}_{J+2N+k,J+\ell}|^2 \mathbf{S}_{f,\ell} \\ &\quad + \sum_{\ell=1}^N |\mathbf{G}_{J+2N+k,J+N+\ell}|^2 \mathbf{S}_{V_n,\ell} + \sum_{\ell=1}^N |\mathbf{G}_{J+2N+k,J+2N+\ell}|^2 \mathbf{S}_{V_r,\ell} + \mathbf{S}_W^k \end{aligned} \quad (29)$$

and this has to be compared with the spectral density of the k -th SQUID input current due to the GW. This last quantity is obtained as the square of the equ. (27) and reads

$$S_k^{GW} = \frac{1}{4} \omega^4 m_s^2 R_s^2 \chi^2 \left| \sum_{\ell m} \mathbf{G}_I^{k\ell} \mathbf{T}_V^{\ell m} \left(\frac{\tilde{h}_+}{\tilde{h}_\times} \right)^m \right|^2 \quad (30)$$

If we know the GW arrival direction we can compute each \mathbf{T}_V and simulate the detector's response. The inverse problem, computing the GW propagation direction, needs high signal to noise ratio (SNR) [14]. If we are interested in the detector's sensitivity we are working at SNR=1 and therefore have no information on the arrival direction. Furthermore, if we choose an arbitrary direction we can be in a case where some of the modes are poorly or not at all coupled to this peculiar GW and consequently we can underestimate the detector's sensitivity [23]. As the spectral density is a statistical feature of the signal, it is then natural to perform an average on the possible arrival directions and over the polarizations.

Averaging S_k^{GW} the arrival direction and the polarization and assuming $\tilde{h}_+ \equiv \tilde{h}$, $\tilde{h}_\times \equiv 0$ we find [15]

$$S_k^{GW} = \frac{1}{10} \omega^4 m_s^2 R_s^2 \chi^2 \tilde{h}^2 \sum_{\ell=1}^5 \mathbf{G}_{J+2N+k,\ell}^2 \quad (31)$$

The strain sensitivity is given by the comparison $S_{I_i^k} = S_k^{GW}$ and is

$$\tilde{h}_c(\omega) = \left(\frac{S_{I_i^k}}{\frac{1}{20} \omega^4 m_s^2 R_s^2 \chi^2 \sum_{\ell=1}^5 \mathbf{G}_{J+2N+k,\ell}^2} \right)^{1/2} \equiv \left(\frac{S_{I_i^k}(\omega)}{T_F(\omega)} \right)^{1/2} \quad (32)$$

where we have defined the transfer function.

B. Coherent analysis

Rather than looking at each transducer separately we can perform a coherent analysis taking into account all the N signal. From [14] we know that the SNR after optimal filtering

is given by

$$SNR = \int_{-\infty}^{\infty} \sigma(\omega) d\omega / 2\pi \quad (33)$$

$$\sigma(\omega) = \mathbf{I}_{\text{sig}}^\dagger(\omega) \mathbf{S}^{-1}(\omega) \mathbf{I}_{\text{sig}}(\omega) \quad (34)$$

Using the expressions (27) we derived in the previous section we get

$$\sigma(\omega) = \frac{1}{4} \omega^4 m_s^2 R_s^2 \chi^2 \begin{pmatrix} \tilde{h}_+^* & \tilde{h}_\times^* \end{pmatrix} \mathbf{T}_V^\dagger \underbrace{\hat{\mathbf{G}}_I^\dagger \mathbf{S}^{-1} \hat{\mathbf{G}}_I}_{\mathbf{H}} \mathbf{T}_V \begin{pmatrix} \tilde{h}_+ \\ \tilde{h}_\times \end{pmatrix} \quad (35)$$

In order to evaluate this expression we face again the problem that \mathbf{T}_V is a function of the arrival direction and of the polarization of the GW. As in the single transducer analysis it is then convenient to average the expression over the direction and the polarization. This gives

$$\begin{aligned} \langle \begin{pmatrix} \tilde{h}_+ \\ \tilde{h}_\times \end{pmatrix}^\dagger \mathbf{T}_V^\dagger \mathbf{H} \mathbf{T}_V \begin{pmatrix} \tilde{h}_+ \\ \tilde{h}_\times \end{pmatrix} \rangle &= \int_0^\pi \int_0^{2\pi} \frac{\sin(\theta) d\theta d\phi}{4\pi} \int_0^\pi \frac{d\psi}{\pi} \begin{pmatrix} \tilde{h}_+ \\ \tilde{h}_\times \end{pmatrix}^\dagger \mathbf{T}_V^\dagger \mathbf{H} \mathbf{T}_V \begin{pmatrix} \tilde{h}_+ \\ \tilde{h}_\times \end{pmatrix} \\ &= \frac{1}{5} \text{Tr}(\mathbf{H}) (\tilde{h}_+^2 + \tilde{h}_\times^2) \end{aligned} \quad (36)$$

assuming again a non polarized GW $\tilde{h}_+ \equiv \tilde{h}$, $\tilde{h}_\times \equiv 0$ we get for $\langle \sigma \rangle$

$$\langle \sigma \rangle(\omega) = \frac{1}{20} \omega^4 m_s^2 R_s^2 \chi^2 \tilde{h}^2 \text{Tr}(\mathbf{H}) \quad (37)$$

The strain sensitivity (averaged on the sky and polarization) is then given by solving the equation $\langle \sigma \rangle(\omega) \equiv 1$ for $\tilde{h}(\omega)$. We eventually obtain

$$\tilde{h}_c(\omega) = \frac{2\sqrt{5}}{\omega^2 M_s R_s \chi \sqrt{\text{Tr}(\mathbf{H})}} \quad (38)$$

VI. SIMULATION RESULTS

A. Filled sphere

With a numerical code, implementing (6),(9-18),(29), (32)and (38), we can compute the strain sensitivity for a spherical resonant mass with capacitive transducers coupled to a dc-SQUID with input transformer and resonances frequency of the transducer tuned to the five quadrupolar modes.

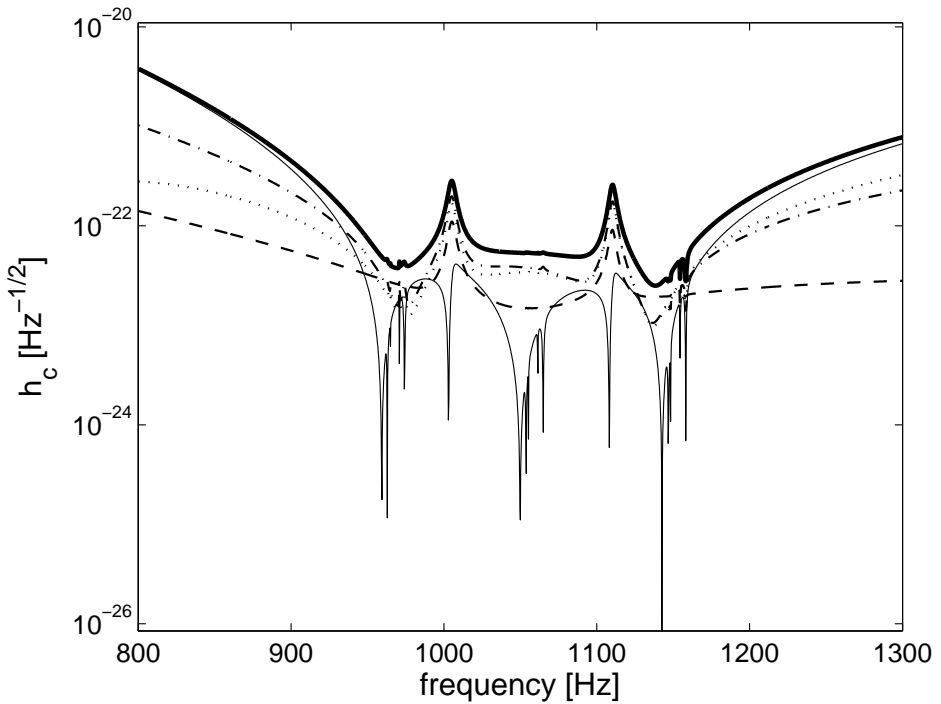


FIG. 3: Strain sensitivity at the quantum limit for one of the 6 transducers placed into a TIGA configuration on a 1[m] radius bulk CuAl sphere. The curves are the relative contributions of the different noises: the thick line is the total sensitivity, the dashed curve is the mechanical thermal noise contribution (14,15), the dashed-dotted line is the thermal electric noise contribution (16), the dotted line the back-action contribution (17) and the continuous curve the white noise (18).

1. Single transducer results

In the case of a single transducer analysis, we obtain N sensitivity curves – one for each transducer. As an example we considerate a 1[m] radius bulk CuAl sphere with 6 transducers in TIGA configuration. At the quantum limit, the typical strain sensitivity of one of the transducers is plot in figure 3. Note the presence of horns on the both side of the resonance. We can understand these horns as the contribution from the noises of the 5 others transducers. This explanation is confirmed by the sensitivity curves obtained for the same sphere but with a different number of transducers, see figure 4. As we increase the number of transducers we also increase the number of noises sources and the sensitivity of a single transducer is worse than if the sphere is equipped with a single transducer.

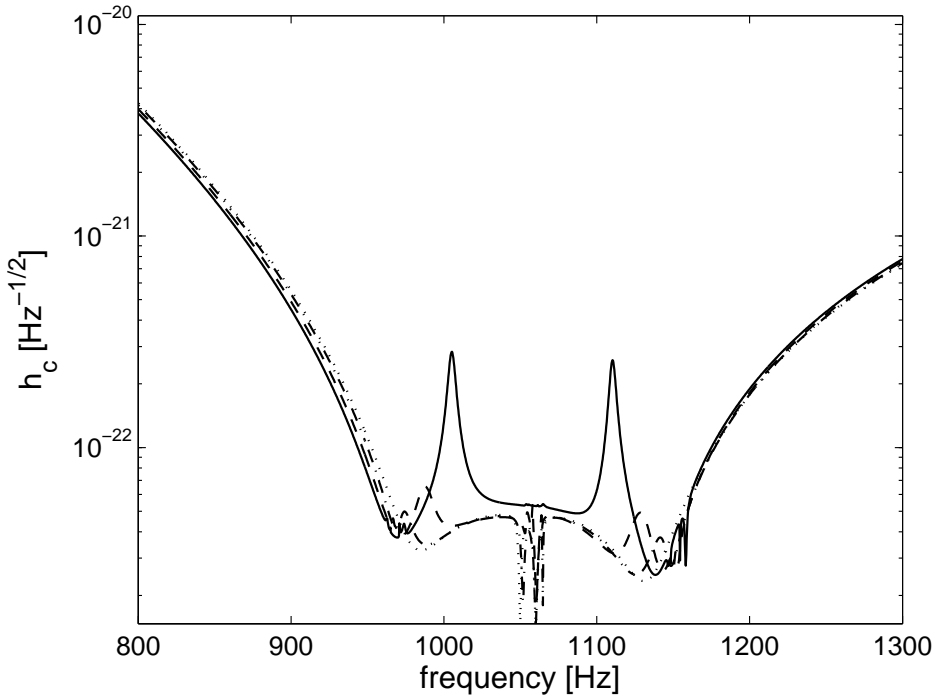


FIG. 4: Strain sensitivity at the quantum limit for one transducers of a transducer set placed on a 1[m] radius bulk CuAl sphere. The continuous curve is the sensitivity for a transducer out of a 6 transducer TIGA configuration, the dashed curves the one for a set of 4 transducers on the 4 first TIGA location the dashed-dotted curves the one for a set of 2 transducers on the 2 first TIGA location and the dotted curve is for a single transducer .

2. Coherent analysis results

We now work out the coherent strain sensitivity for the same sphere as in the previous case. For 6 transducers placed into a TIGA configuration the sensitivity is now free of horn and is show in figure 5. We also plot the sensibility corresponding to the best present transducer ($N_{phonon} = 50$).

In the case of the coherent analysis adding a transducer improve the sensitivity as it is show in the figure 6.

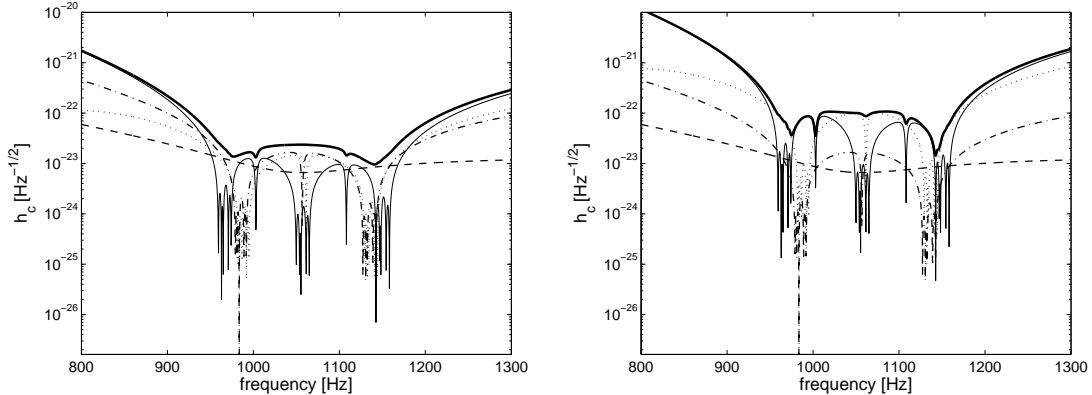


FIG. 5: Strain sensitivity at the quantum limit (left) and for $N_{phonon} = 50$ (right) for a coherent analysis of the outputs of 6 transducers placed into a TIGA configuration on a 1[m] radius bulk CuAl sphere. The curves are the relative contributions of the different noises: the thick line is the total sensitivity, the dashed curve is the mechanical thermal noise contribution (14,15), the dashed-dotted line is the thermal electric noise contribution (16), the dotted line the back-action contribution (17) and the continuous curve the white noise (18).

B. The hollow sphere

All the above treatment has a nice, simple generalization to the case of a hollow sphere [16]. While preserving all the feature of a bulk sphere such as omni-directionality, and the capability to determine the source direction and wave polarization, an hollow sphere has several interesting peculiar properties. Its quadrupole frequencies are lower than those of an equally massive solid sphere, thus making the low-frequency range accessible to this antenna with good sensitivity. Further, as shown in [16], for an appropriate ratio between the inner and outer diameter, the cross section for the second quadrupole mode equals that of the first, and one has the possibility of working with a detector with the same (high) sensitivity at two frequencies. One could for example in this way study the radiation emitted by a binary system, consisting of either neutron stars or black holes, in the inspiral phase and determines the chirp mass by measuring the time delay between excitations of the first and second quadrupole modes of an hollow sphere. We have investigated the system response of an hollow sphere to the classical GW signal. Essentially the only differences with the bulk sphere are the numerical values of the radial functions α_j that we first met in equation

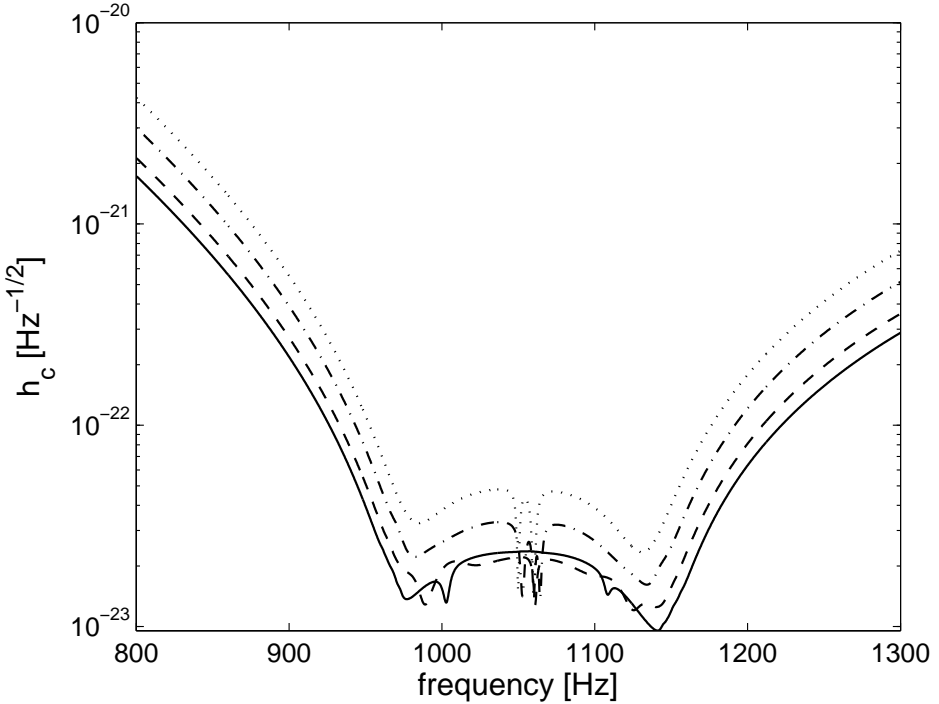


FIG. 6: Coherent strain sensitivity at the quantum limit of a transducer set placed on a 1[m] radius bulk CuAl sphere. The continuous curve is the sensitivity for a 6 transducers TIGA configuration, the dashed curves the one for a set of 4 transducers on the 4 first TIGA location the dashed-dotted curves the one for a set of 2 transducers on the 2 first TIGA location and the dotted curve is the sensitivity for a single transducer . (Note that the dotted curve is the same as in figure 4)

(3), and the one of the coupling to GW, namely χ (see equation (25)). We have also to recompute the eigen-frequencies. In figure 7 we show the coherent strain sensitivity at the quantum limit for a CuAl sphere with 1[m] external radius and 0.4[m] internal radius, when 6 transducers in the TIGA configuration are coupled to the first quadrupolar modes.

The total sphere mass is of about 30 tons. The noise contributions are the same considered for the full sphere. In Fig. 7 the sensitivity for the best present transducer is also shown. Further we calculate the sensitivity of the hollow sphere when two sets of 6 transducers are placed in the TIGA configuration and coupled respectively with the first and second quadrupolar modes.

Because the radial displacement of the second mode is maximum at the inner side of the sphere [16], one can enhance the sensitivity by mounting the classical capacitive transducers

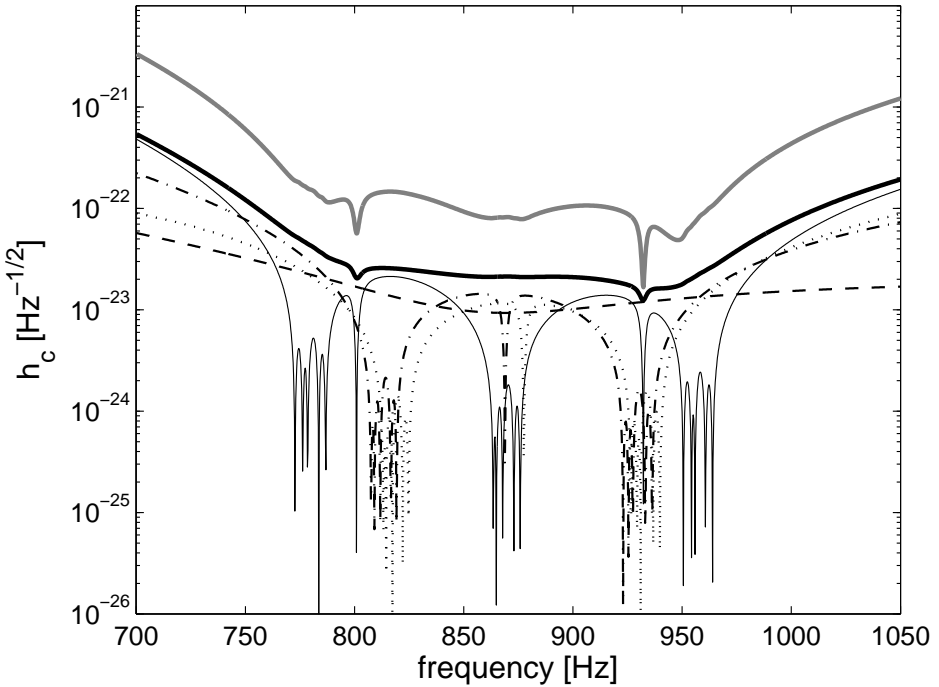


FIG. 7: Coherent strain sensitivity at the quantum limit for a set of 6 transducers placed in a TIGA configuration on a $0.4[m]/1[m]$ internal/external radius CuAl sphere. The curves are the relative contributions of the different noises (see figure 3). The gray curve is the sensibility corresponding to the best present transducer ($N_{phonon} = 50$).

considered here inside the sphere. However the increase of the experimental complexity of the detector due to the presence of transducers inside the sphere has to be put into balance with the sensitivity gain for such a configuration (mostly in the bandwidth which pass from 20 Hz for transducers outside to 200 Hz for the inside position, see the right panel of Fig. 8). According to present technology, we show the details of the sensitivity computed with the second set of transducers attached at the outer side of the hollow sphere.

The large total number of transducers and read-out electronics would contribute as well to the detector complexity. In a following paper we will discuss a possible simpler read-out scheme, which will reduce the number of SQUID and electronics necessary for each transducer signal amplification [6].

Fig. 8 shows the sensitivity of a hollow sphere equipped with 2×6 capacitive transducers coupled to the first and second quadrupolar modes. The detector is equally sensitive at

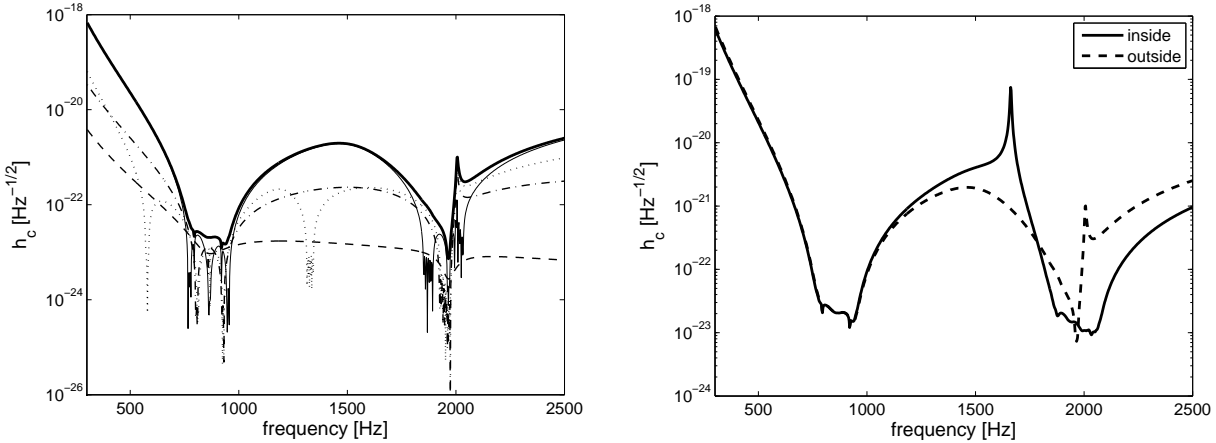


FIG. 8: Left panel: coherent strain sensitivity at the quantum limit for two sets of 6 transducers placed in a TIGA configuration on a $0.4[\text{m}]/1[\text{m}]$ internal/external radius CuAl sphere. Each transducer set is coupled to the first and second quadrupolar modes, respectively. The curves show the relative contributions of the different noises: the thick line is the total sensitivity, the dashed curve is the total mechanical thermal noise contribution (14,15), the dashed-dotted line is the thermal electric noise contribution (16), the dotted line the back-action contribution (17) and the continuous curve the white noise (18). The right panel shows the sensitivity gain obtained by mounting the second set of transducer inside the sphere (continuous curve) with respect to the outer transducer configuration (dashed curve).

850 Hz and 2000 Hz and has a total bandwidth of about 200 Hz . With an appropriate resizing of the sphere, the second quadrupolar modes can be shifted to the frequency region where existing small spherical detectors are sensitive. This would open the possibility of coincidence search between several spherical detectors and the DUAL detector [17], building in this way the base for a powerful omni-directional gravitational wave observatory.

C. Effect of the thickness of the hollow sphere

We address now the question of the influence of the thickness of the sphere. For a fixed external radius a thinner sphere is less massive and therefore less sensitive. There is also a shift in the resonances to lower frequencies, see figure 9. Only the first quadrupolar mode is considered for simplicity. We remark that for a detector with sensitive resonances as low as 400 Hz a active mechanical damping system would probably be required to reduce external

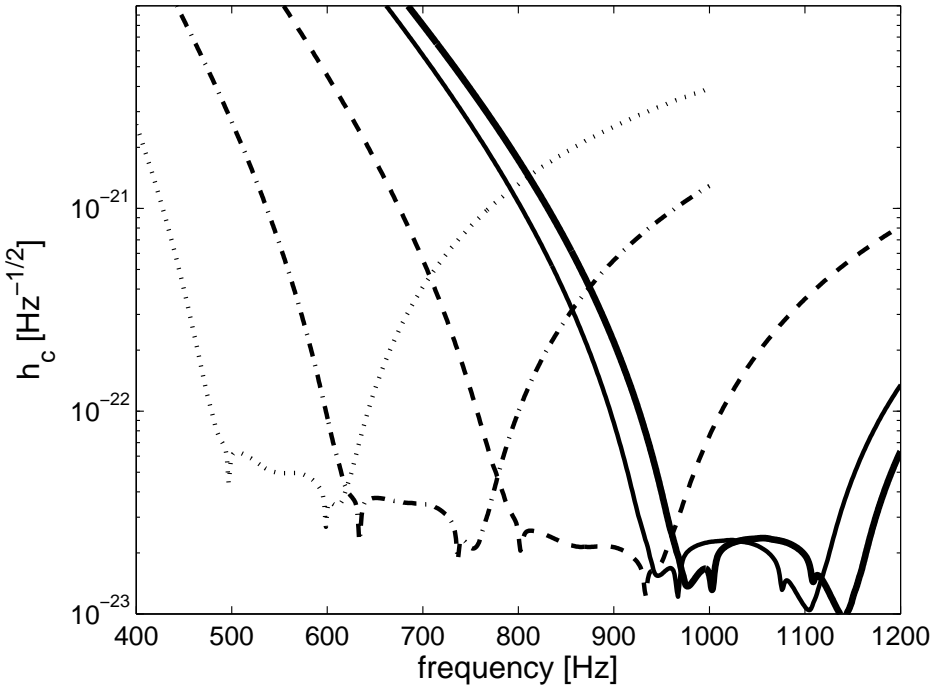


FIG. 9: Coherent strain sensitivities at the quantum limit for a TIGA configuration on a 1[m] external radius hollow CuAl sphere for different values of the internal radius a . The dotted curve is for $a = 0.8[m]$ (ie. a shell of thickness 0.2[m]) the successive curves are for a decreased by step of 0.2[m] until the black thick line which stand for the filled sphere.

mechanical vibration in this frequency region.

VII. CONCLUDING REMARKS

We have shown how to build models giving the strain sensitivity of a GW spherical detector and presented different possibilities of a multi-mode spherical resonant detector. As an example a 1[m] radius CuAl sphere has a peak sensitivity comparable with the first generation of interferometers but is also able to determine the GW arrival direction.

We discussed the sensitivity of a hollow sphere when both the first and second quadrupolar mode are monitored. A hollow sphere could have a sensitivity comparable with future large full spherical detector and a total bandwidth of about 400 Hz in the range of 800 Hz and 2.5 kHz .

Acknowledgments

Simulations have been performed using the Matlab software.

We wish to acknowledge M. Maggiore, S. Foffa, M.A. Gasparini, C. Caprini and A. Malaspinas for many useful discussions.

The work of F.D. and J.E. is partially supported by the Fonds National Suisse. The work of L.G. was partially supported by the Integrated Large Infrastructures for Astroparticle Science (ILIAS) of the Sixth Framework Program of the European Community when the author was employed at Leiden University.

- [1] ALLEGRO - gravity.phys.lsu.edu , AURIGA - www.auriga.lnl.infn.it ,
MARIO SCHENBERG - www.das.inpe.br/~graviton/English ,
MiniGRAIL - www.minigrail.nl , ROG - www.lnf.infn.it/esperimenti/rog/index.html ,
GEO - www.geo600.uni-hannover.de , LIGO -www.ligo.caltech.edu ,
LISA - lisa.jpl.nasa.gov , TAMA - tamago.mtk.nao.ac.jp ,
VIRGO - www.virgo.infn.it
- [2] IGEC - <http://igec.lnl.infn.it> , LIGO-TAMA - ArXiv:gr-qc/0512078
- [3] See for example: B. Abbott et al. (LSC), Phys. Rev. D 72, 042002 (2005).
- [4] L. Baggio et al, Phys. Rev. Lett. 94 (2005) 241101.
- [5] S.M. Merkowitz and W.W. Johnson, Phys. Rev. D **51**, 2546 (1995)
S.M. Merkowitz and W.W. Johnson, Phys. Rev. D **56**, 7513 (1997)
- [6] F. Dubath, J. Extermann, L. Gottardi, In preparation.
- [7] C. Frajuba et all, Class.Quant.Grav.21 (2004) S1107-S1111.
- [8] A. de Waard et al, Class.Quant.Grav.22, S215 - S219 (2005).
- [9] P.F. Michelson and C.Y. Zhou, Phys. Rev. D **51**, 2517 (1994)
- [10] L. Gottardi, Transducers and low noise two-stage SQUID amplifiers for the spherical gravitational wave antenna MiniGRAIL, PhD thesis, Lion, Universiteit Leiden, Nederland (2004),
L. Gottardi, submitted to Phys. Rev. D (2006) - ArXiv:gr-qc/0608097
- [11] Tesche, CD and Clarke, J., J. Low Temp. Phys. **29**, 301 (1977).
Tesche, CD and Clarke, J., J. Low Temp. Phys. **37**, 397 (1979)

- [12] M. A. Gasparini, Phys. Rev. D **72**, 104012 (2005).
- [13] M. Maggiore, “Gravitational Waves, Vol I, Theory and Experiments”, Oxford University Press, to appear.
- [14] T.R. Stevenson, Phys. Rev. D **56**, 7513 (1997)
- [15] J. Extermann, Sur la sensibilité d'une masse résonnante sphérique comme détecteur d'ondes gravitationnelles, diploma thesis, Université de Genève (2005)
- [16] E. Coccia, V. Fafone G. Frossati, J.A. Lobo and J.A. Ortega, Phys. Rev. D **57**, 2051 (1998).
- [17] M. Bonaldi et al, Phys. Rev. D **74**, 022003 (2006).
- [18] We use j to describe collectively all the numbers needed to specify the mode. For spheroidal modes $j=\{n, l, m\}$, see [5].
- [19] The precise location of the transducer just changes the B matrix.
- [20] As we have only modes with $l = 2$, all the α_j are equal. Therefore, we drop the indices.
- [21] By a GW tensor we mean the perturbation of the background metric in the TT gauge
- [22] Note that if we describe gravitation by general relativity, only spheroidal quadrupolar modes ($l = 2$) have non zero \tilde{h}_j .
- [23] As an illustration in the case of a cylindrical detector. If we choose the GWs arrival direction parallel to the detector axis, the GW is not seen and no information is given about the detector sensitivity.